Structure and Properties of Styrene-Butadiene Rubber (SBR) with Pyrolytic and Industrial Carbon Black

P. Berki, R. Göbl and J. Karger-Kocsis*

Department of Polymer Engineering, Faculty of Mechanical Engineering, Budapest University of Technology and Economics, and MTA-BME Research Group of Composite Science and Technology, H-1111 Budapest, Muegyetem rkp. 3, Hungary

Authors' e-mails: karger@pt.bme.hu (*corresponding), berki@pt.bme.hu, richard.gobl@outlook.com

ABSTRACT

To evaluate the performance of pyrolytic carbon black (pCB), we filled styrene-butadiene rubber (SBR) with pCB and N330 industrial carbon black (CB). We used two ratios of pCB and N330: 1/9 and 1/1. N330 was selected because its specific surface area was close to that of pCB. The overall CB content in the mixes was 0, 30, 45 and 60 part per hundred rubber (phr). We studied the effects of types and amounts of CB on the dispersion, cure behavior, dynamic mechanical thermal behavior, tensile mechanical and fracture mechanical properties of the filled rubbers. Dispersion of pCB was poorer than that of N330 CB. With respect to tensile mechanical properties – except tear strength – N330 outperformed pCB. The tear strength and fracture mechanics characteristics (J-integral at crack tip opening, and trouser tear strength) of SBR were higher with pCB than with N330. This can be attributed to the broader dispersion of pCB than N330. The combined use of N330 and pCB resulted in intermediate values reflecting the actual N330/pCB ratio for all measured parameters. We wanted to correlate the mechanical performance with the apparent molecular weight between crosslinks (M_c), and found reasonable correlations for the Payne effect, tensile strength and critical J-integral. On the other hand, we only found a tendency for tear characteristics; this was ascribed to additional effects of (p)CB dispersion.

Keywords:

styrene-butadiene rubber; pyrolytic carbon black; mechanical properties; J-integral; structure-property relationship; apparent molecular weight between crosslinks

1. INTRODUCTION

The disposal of waste tires is a global environmental problem and their economic recycling is a great challenge. Retreading worn tires has severe limitations (residual profile depth) and burning tires to generate heat is less straightforward. The recycling of used tires is hampered by their complex structure (various rubbers and fillers and steel cord reinforcement). Ground tire rubber (GTR), which is another option for recycling, is available from different sources (car tires, truck tires etc.). However, the traditional application field of GTR (covers of sporting fields and play grounds) is saturated, therefore, considerable efforts are made to convert GTR into other value added products. Reclaimed GTR, by whatever means achieved, may be used in fresh rubber mixes [1, 2]. The production of thermoplastic rubbers with the use of GTR is strongly preferred, though this requires some "activation" (e.g. devulcanization/polymerization) of the GTR particles [3]. Nowadays, the preferred method for that is microwave devulcanization [4-7]. Another product that can be made from used tires is pyrolytic carbon black (pCB), which has been attracting more and more interest lately. pCB can be produced in relatively high yield (ca. 35 wt.%) through various pyrolysis processes of used tires [8, 9]. Other pyrolytic products are gas and oil. The former is usually used in a closed loop as fuel to maintain the pyrolysis process. Pyrolytic oil with and without further purification may also have commercial value, even as extender oil for rubbers [10]. pCB itself may be considered as a "green" (i.e. recycled CB) filler of rubbers. There are already several reports on the applicability of pCB in rubbers, including natural rubber (NR) [11], styrene-butadiene rubber (SBR) [12-14], and NR+SBR combinations [15]. Thus, pCB of controlled quality may be added to tires and other rubber compounds, thereby partially or fully replacing industrial CBs. An important finding of papers on the use of pCBs of various origins in different rubber mixes is that their properties are close to those of industrial reinforcing and semi-reinforcing furnace CBs in the range of N300 to N700 [13, 14].

The reinforcing effect of pCB should be examined in a "green" rubber without self-reinforcement. This criterion is well met by SBR, which is always filled to achieve the required performance (unfilled SBR has poor mechanical and wear properties) [16]. Moreover, SBR and NR are the major rubber ingredients of tire recipes. Our goal was to compare the reinforcing properties of pCB with an industrial CB whose specific surface area is close to that of pCB. N330 CB fulfils this requirement and was therefore selected for benchmarking. N330, pCB and their combinations in 9/1 and 1/1 ratios were added to SBR in amounts of 30, 45 and 60 part per hundred rubber (phr). We investigated whether the specific surface area is the control parameter of pCB classification and its performance. A further aim of this work was to check

how mechanical and fracture mechanical properties change as a function of apparent molecular weight between crosslinks (M_c).

2. EXPERIMENTAL

2.1.Materials

We chose SBR 1502 (styrene content: 23.5%, Mooney viscosity ML (1+4) at 100 °C: 48 MU) of Sterlitamak JSC, Russia, as rubber. The characteristics of the pelletized pyrolytic carbon black (pCB) are as follows: carbon content ≈80 wt%, silica content ≈13 wt% and specific surface area (nitrogen, BET): ≈75 m^2/g [14]. The corresponding properties of the industrial N330 CB (provided by Tauril Co., Hungary) are: carbon content ≈ 99.5 %, specific surface area ≈ 80 m^2/g. Sulfuric curable SBR mixes with different amounts of carbon black were prepared (see Table 1).

Table 1: The designation codes and compositions of the SBR mixes studied. MBTS: 2'-dibenzothiazole disulfide

Designation	Composition [phr]							
	SBR	∑ CB	N330	pCB	ZnO	Stearic acid	MBTS	S
SBR ref.	100	-	-	-	3	2	1.5	2
30N330	100	30	30	-	3	2	1.5	2
30(N330/pCB=9/1)	100	30	27	3	3	2	1.5	2
30(N330/pCB=1/1)	100	30	15	15	3	2	1.5	2
30pCB	100	30	-	30	3	2	1.5	2
45N330	100	45	45	-	3	2	1.5	2
45(N330/pCB=9/1)	100	45	40.5	4.5	3	2	1.5	2
45(N330/pCB=1/1)	100	45	22.5	22.5	3	2	1.5	2
45pCB	100	45	-	45	3	2	1.5	2
60N330	100	60	60	-	3	2	1.5	2
60(N330/pCB=9/1)	100	60	54	6	3	2	1.5	2
60(N330/pCB=1/1)	100	60	30	30	3	2	1.5	2
60pCB	100	60	-	60	3	2	1.5	2

2.2.Compounding and curing

The rubber was mixed on a laboratory two-roll mill (LRM-SC-110, Labtech Engineering Co., Ltd., Thailand). Friction was set to 1.3 and the temperatures of the front and back rotors were 70°C and 50°C, respectively. The additives were introduced from the 5th to the 20th min after mixing was started. Total mixing time was 25 min. The samples were cured in a Teach-Line Platen Press 200E laboratory press (Dr. Collin GmbH, Germany) at 160°C for $t_{0.9}$ (the time needed to reach 90% of curing – see later) of the compounds with 5 MPa pressure, producing sheets with a thickness of 2 mm.

2.3.Testing

Curing

The curing of the samples was examined with a Monsanto R100S rheometer, (MonTech Werkstoffprüfmaschinen GmbH, Germany) in isothermal time sweep mode (1,667 Hz, 1° angle) at T=160°C for 45 minutes.

CB dispersion

Specimens were cut, embedded in polyester resin and polished in five steps (coarse SiC, P320, P1000; fine SiC, P2000, P4000 and 1 μm diamond suspension). Macrodispersion was assessed with an Olympus BX51M light microscope, equipped with a DP26 digital camera (Olympus GmbH, Germany) at a magnification of 105x in reflected light. The captured images (about ten per sample) were evaluated with the Olympus Stream software. In the macrodispersion examination the software was set to perceive particles with a diameter of >1 μm as particles. The dispersion coefficient was calculated by dividing the total cross-sectional area of the macroparticles with the view field area at this magnification, multiplying it by 100 and subtracting it from 100%.

(p)CB dispersion was also assessed with atomic force microscopy (AFM) – NanoSurf FlexAFM 5 (Nanosurf AG, Switzerland). The phase contrast images (25 μm x 25 μm) were prepared in tapping mode with the use of a TAP190 AL-G type cantilever.

Dynamic-mechanical thermal analysis (DMTA)

DMTA spectra were registered on rectangular specimens in tensile mode at a static preload of 0.1 N with a superimposed sinusoidal 0.1% strain. The frequency was 10 Hz and the spectra were taken in a temperature range of -100 to 70°C using a Q800 device of TA Instruments Co. (USA). The temperature ramp was 3°C/minute. DMTA was used to assess the Payne effect. It was also investigated in tensile mode, at a static preload of 0.01N at 30 °C with a frequency of 10 Hz and a strain sweep from 0.01 to 10% (denoted as M0.01 and M10, respectively).

Mechanical and fracture mechanical tests

Hardness was determined on the prepared sheets with ten measurements on each material according to the DIN 53505 standard. A Zwick H04.3150 hardness tester (Zwick GmbH & Co. KG, Germany) was used with a Shore A measuring head and a load of 12.5 N.

DIN 53504 Type 1 specimens for tensile and ASTM D624 Type C specimens for tear tests were punched from the vulcanized sheets. Tensile and tear tests were performed on a Zwick Z250 universal testing machine equipped with a 20 kN load cell with a crosshead speed of 500 mm/min at room temperature. Each of above tests was repeated on five specimens and the average of the results was calculated.

Fracture mechanical tests were performed on single edge-notched tensile loaded (SEN-T) and trouser tear specimens. SEN-T specimens with dimensions of 100 mm x 25 mm x 2 mm (length x width x thickness) with an initial notch length of 10 mm were loaded at a crosshead speed of

10 mm/min on the above-mentioned Zwick testing machine. Nowadays researchers pay more attention to the investigation of crack propagation and the failure process in addition to fracture mechanical properties. We applied crack tip opening displacement (CTOD) to study crack propagation. It was followed by visual inspection with a digital microscope (Dino-Lite Premier AM4113ZT (R4), New Taipei City, Taiwan). The camera was positioned in front of the crack in order to focus on the internal surface generated by the blunting and/or growth of the crack. Prior to this test, the crack surfaces were coated with talc (in the case of the unfilled SBR coating was done with pCB) for contrast. By analyzing the sequence of images, we were able to detect the point where fracture started to propagate, and calculated the corresponding J-integral [17, 18]:

$$J = \frac{\eta \cdot U}{t \cdot (W - a)} \tag{1}$$

where η is a geometry factor (0.9 in this case), U is the input energy (area under the load-displacement curve up to the point considered), t is the thickness (≈2 mm), while W is the width (25 mm) of the specimen, and a is initial crack length (10 mm). The J-integral was displayed as a function of crack tip opening displacement (CTOD). The critical value of the J-integral, assigned to crack initiation, was read at a CTOD of 0.1 mm. This threshold criterion is widely used [19, 20]. Since Mullins-softening may have an influence on the fracture mechanical response [14], J-CTOD curves were also obtained from testing cyclically preloaded specimens. Cyclic preloading up to 100% deformation in five consecutive cycles was performed prior to notching the SEN-T specimens. Further details of this test can be seen in Refs. [14, 19].

The fracture energy of the trouser tear test ($J_{trouser}$) was determined on 100 x 30 x 6mm (length x width x thickness) waisted specimens (i.e. the thickness of the specimen in the anticipated crack growth was 1 mm, whereas the legs were 6 mm thick) with an initial notch length of 40 mm at a deformation rate of 100 mm/min via Eq. 2 [21]:

$$J_{trouser} = \frac{2 \cdot F_{tear}}{t}, \tag{2}$$

where F_{tear} is the mean force during stable tearing, and t is the thickness of the specimen. All fracture mechanics tests were also run on five specimens and the averages were calculated.

3. RESULTS AND DISCUSSION

3.1. Cure behavior

Characteristic vulcanizations curves (e.g. as torque vs. time) are displayed in Fig. 1. Table 2 shows the following data: lowest and highest torque data (M_l and M_h, respectively), times to reach 10, 50 and 90% crosslinking ($t_{0.1}$, $t_{0.5}$ and $t_{0.9}$, respectively) and times to reach 1 and 2 dNm torque above the M_l torque value (t_{s1} and t_{s2}, scorch times). Based on Fig. 1, and the related tabulated data (Table 2) the following tendencies can be observed:

- pCB slightly delays curing compared to N330 at the same CB content

- M_l is lower, while M_h is higher for N330 than pCB at the same CB content. This suggests that N330 is a more active filler than pCB, even though their specific surface area are almost the same.

- a combined use of N330 and pCB results in intermediate values, which are in harmony with the respective N330/pCB ratio

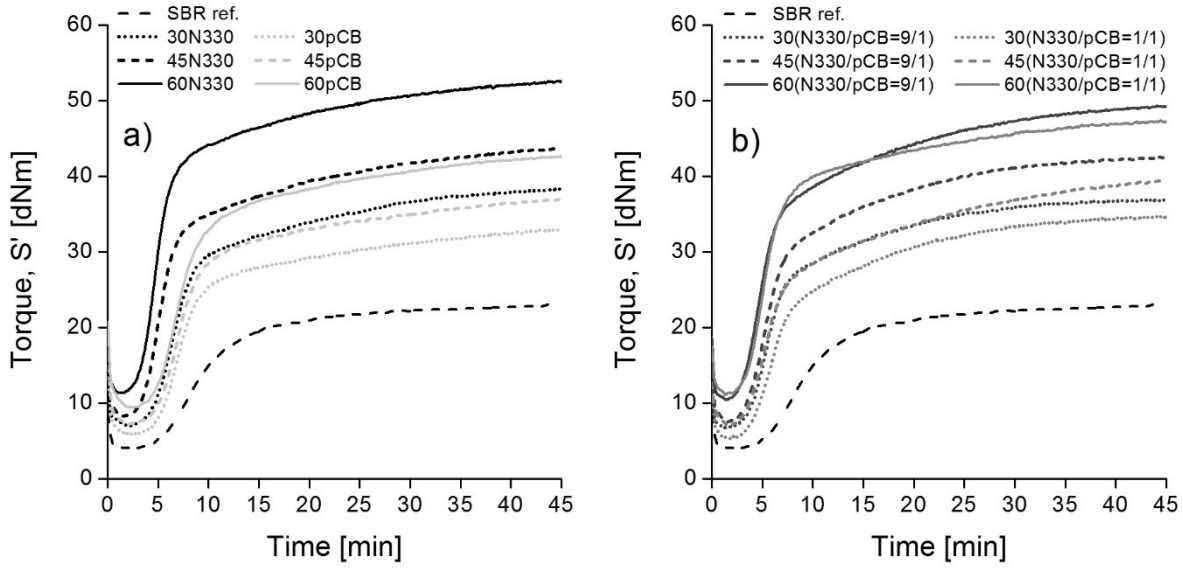

Figure 1: Vulcanization curves of the SBR mixes with N330 and pCB (a) and with N330+pCB (b) at different CB contents

Table 2: Vulcanization results

Designation	M_h [dNm]	M_l [dNm]	$t_{0.1}$ [min]	$t_{0.5}$ [min]	$t_{0.9}$ [min]	t_{s1} [min]	t_{s2} [min]
SBR ref.	23.1	4.0	5.6	9.1	20.6	4.8	5.7
30N330	38.4	7.0	4.7	7.2	24.6	3.7	4.3
30(N330/pCB=9/1)	36.9	6.8	4.0	6.2	21.1	3.1	3.6
30(N330/pCB=1/1)	34.7	5.3	4.2	7.0	23.2	3.3	3.8
30pCB	33.1	5.8	5.2	7.6	25.7	4.2	4.9
45N330	43.7	8.2	3.7	5.7	23.2	2.9	3.3
45(N330/pCB=9/1)	42.6	7.6	3.7	6.1	22.1	2.8	3.3
45(N330/pCB=1/1)	39.6	7.1	3.8	6.5	27.6	2.9	3.4
45pCB	37.0	7.3	5.1	7.6	24.5	3.9	4.7
60N330	52.6	11.3	3.4	5.2	20.2	2.5	2.9
60(N330/pCB=9/1)	49.3	10.5	3.3	5.5	22.9	2.5	2.9
60(N330/pCB=1/1)	47.4	11.1	3.7	5.7	20.8	2.7	3.1
60pCB	42.7	9.4	5.1	7.6	23.7	4.1	4.5

3.2. CB dispersion

Fig. 2 displays characteristic optical microscope images of CB dispersions in the mixes studied. The dispersion coefficients, and average and maximum sizes of the macroparticles are listed in Table 3. The dispersion coefficients of the SBR mixes with N330 are higher than 95%, and the value slightly increases as N330 content increases. The dispersion coefficient values with pCB are markedly lower and they do not depend on pCB content. Therefore, the dispersibility of pCB is poorer than that of industrial N330 CB. The combined use of N330 and pCB yields intermediate dispersion coefficient values, as expected. A similar tendency is true for the mean size of the macroparticles, although particle size has a wider distribution. The maximum size of the macroparticles was usually higher for pCB and N330/pCB than for N330.

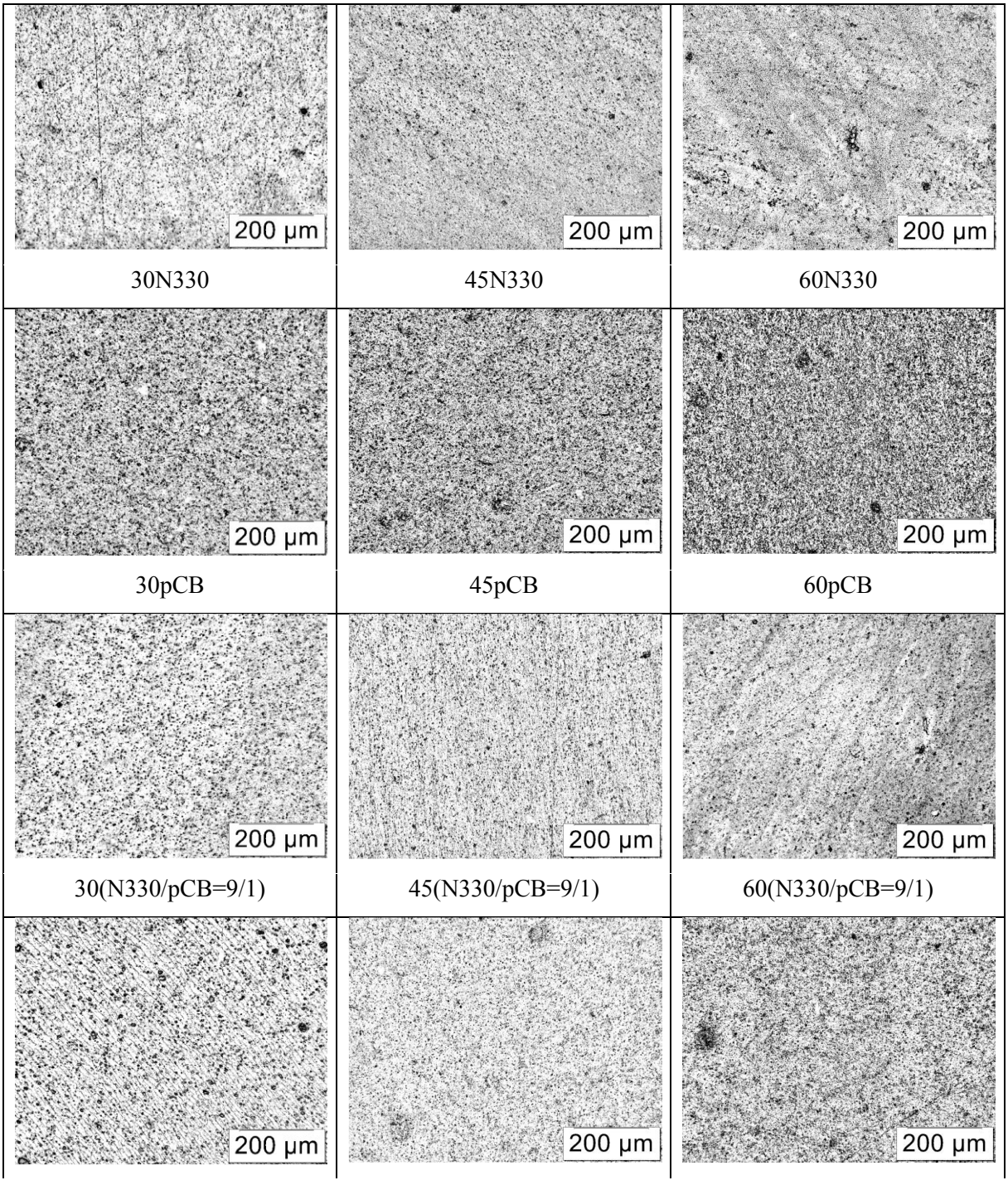

30(N330/pCB=1/1)	45(N330/pCB=1/1)	60(N330/pCB=1/1)

Figure 2: Characteristic light microscopy images of the polished surfaces of the SBR mixes

Table 3: Dispersion characteristics of the SBR mixes. Note: it was assumed that the particles have a spherical shape

Designation	Dispersion coefficient [%]	Maximum particle diameter [µm]	Mean particle diameter [µm]
SBR ref.	-	-	-
30N330	95	14.3	3.2
30(N330/pCB=9/1)	90	14.1	4.0
30(N330/pCB=1/1)	89	24.5	7.6
30pCB	86	17.2	7.9
45N330	97	23.8	2.9
45(N330/pCB=9/1)	97	27.4	2.2
45(N330/pCB=1/1)	95	18.5	2.7
45pCB	88	17.4	4.9
60N330	99	26.3	2.1
60(N330/pCB=9/1)	97	20.9	3.6
60(N330/pCB=1/1)	86	27.5	4.8
60pCB	82	27.8	7.0

AFM scans were expected to confirm the above light microscopy results. Figure 3 compares the structure of mixes with 30, 45 and 60 phr overall (p)CB loading. The size of visible particles is roughly the same as mean particle sizes shown in Table 3.

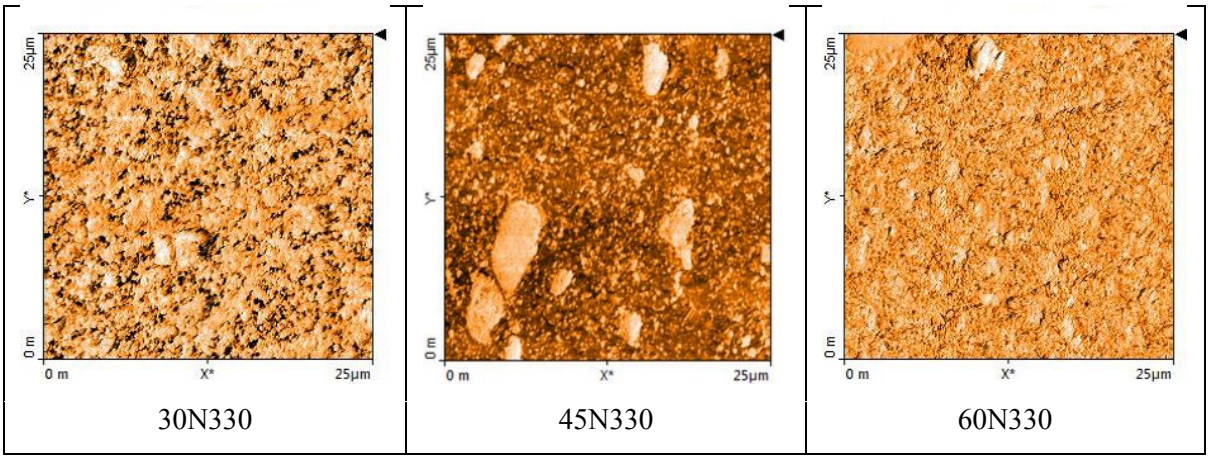

30N330 45N330 60N330

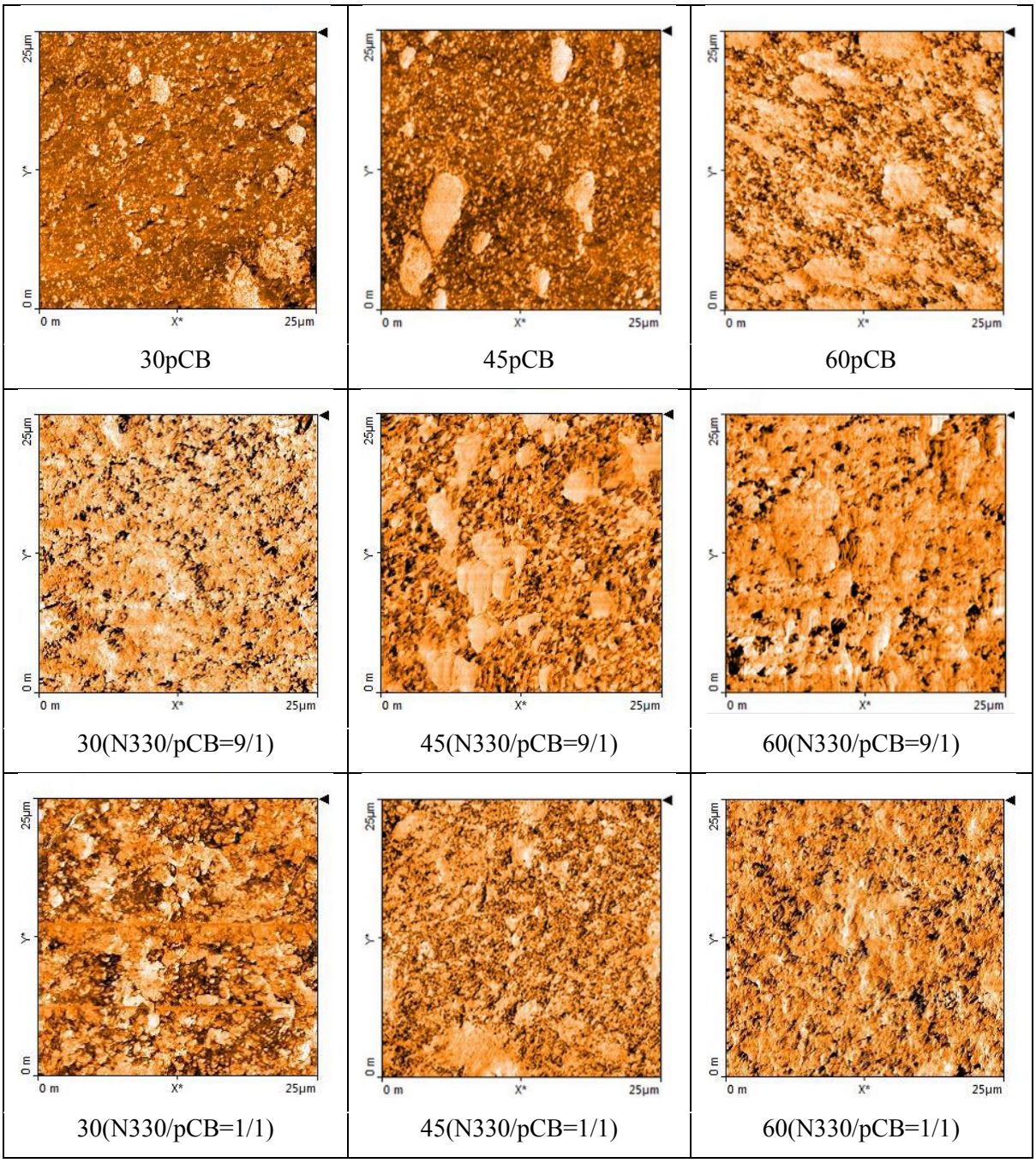

Figure 3: Characteristic AFM phase images taken from the polished surfaces of the SBR mixes

3.3. DMTA behavior

Curves of the storage modulus (E') and mechanical loss factor (tan δ) as a function of temperature are shown for the SBR mixes with the parent and mixed CBs in Figure 4 a) and b). Both glassy and rubbery E' moduli increased with increasing CB content. The increment was always higher for N330 than for pCB (cf. Fig. 4a), which supports the statement that industrial CB is a more active filler than pyrolytic CB. The glass transition temperature (T_g), taken as the temperature of the maximum of the tan δ curve, did not change noticeably as a function of filler

type and amount. The peak value of tan δ was, however, prominently reduced with increasing (p)CB content (cf. Fig. 4). In order to get a deeper insight into structural changes, we further analyzed the DMTA curves. T_g, the rubbery E' moduli ($E_{rubbery}$ read at T_g+30 °C), and the glassy E' moduli (E_{glassy} read at T_g-30°C) values of tan δ were tabulated in Table 4. $E_{rubbery}$ was used to calculate the apparent crosslink density, or more exactly the apparent mean molecular weight between crosslinks, via:

$$M_c = \frac{3\rho \cdot R \cdot T}{E_{rubbery}} \tag{3}$$

where $E_{rubbery}$ is the modulus at $T=T_g + 30K$, ρ is the density (determined in a pycnometer with methanol), R is the universal gas constant (8.314 J/(K.mol), and T is absolute temperature. M_c is an apparent value because in the filled rubbers it is affected by not only their crosslinking but the rubber–filler and filler–filler interactions.

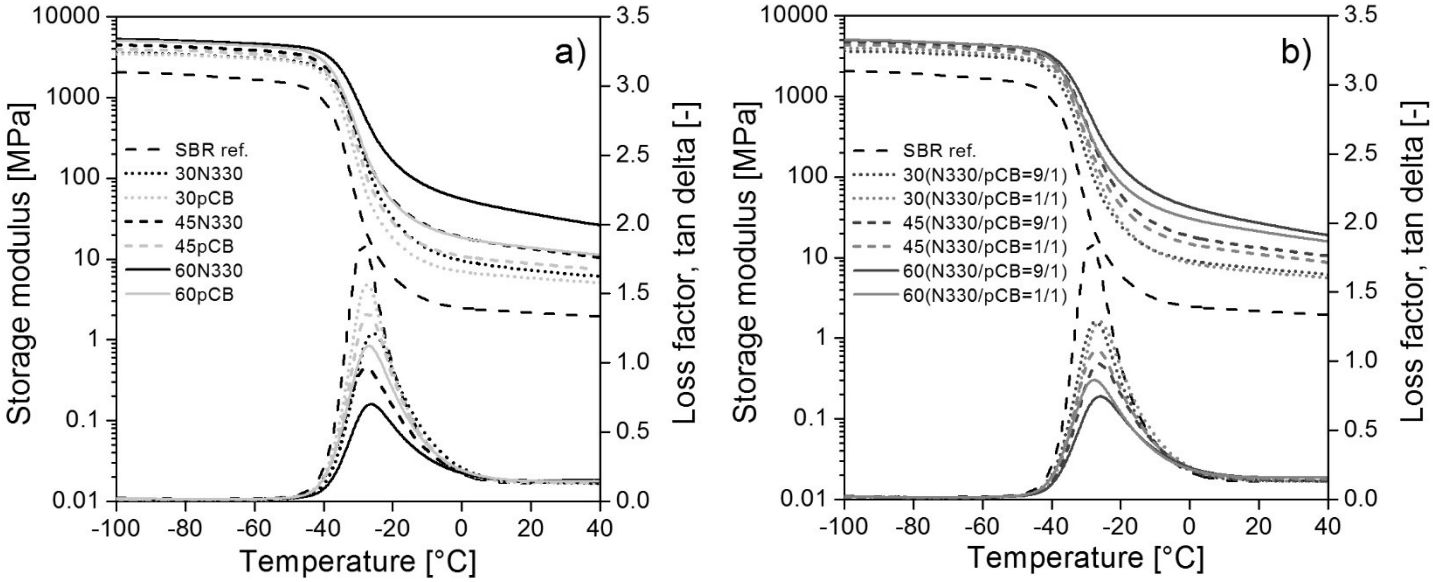

Figure 4: E' and tan δ as a function of temperature and CB content for the SBR mixes with the parent fillers (a) and their combinations (b)

One can see that the value of M_c prominently decreases with increasing CB content, and its value is always lower for mixes with N330 than for pCB. Again, the combined use of N330 and pCB yields intermediate M_c values. This is in line with the former finding that N330 is a more active reinforcement than pCB. The more active CB is and the higher its concentration is, the lower tan δ is. T_g is linked with the segmental motion of the rubber chains in a filler network – this motion is inhibited by increasing CB loading (cf. data in Table 4).

The more developed the filler network is, the stronger the Payne effect is [22]. CB aggregates form agglomerates owing to van der Waals interactions between them. Thus, the Payne effect reflects the agglomeration tendency, or more explicitly the reinforcing activity of a given CB. Figure 5 shows the Payne effect in the investigated strain range for the SBR mixes. The Payne effect is quantified by the difference in the E' moduli measured at 0.01 and 10% tensile strains (denoted as M0.01-M10). As expected, this difference was negligible for the unfilled SBR and

most pronounced for the SBR with N330, especially at 60 phr loading – cf. Figure 5. Again, the combined use of N330/pCB reduced the Payne effect compared to N330. The secondary structure of pCB, controlling the formation of bound rubber, is different from that of industrial CB irrespective of the fact that the specific surface areas of pCB and N330 are comparable (cf. section 2.1).

More can be learnt about the reinforcing efficiency of the fillers when the ratio of the maximum in the loss modulus (E'') to the measured Payne effect (i.e. M0.01-M10) is considered – cf. Table 4. The higher this value is, the more active the actual filler is [13]. These data in Table 4 show that N330 has higher activity than pCB.

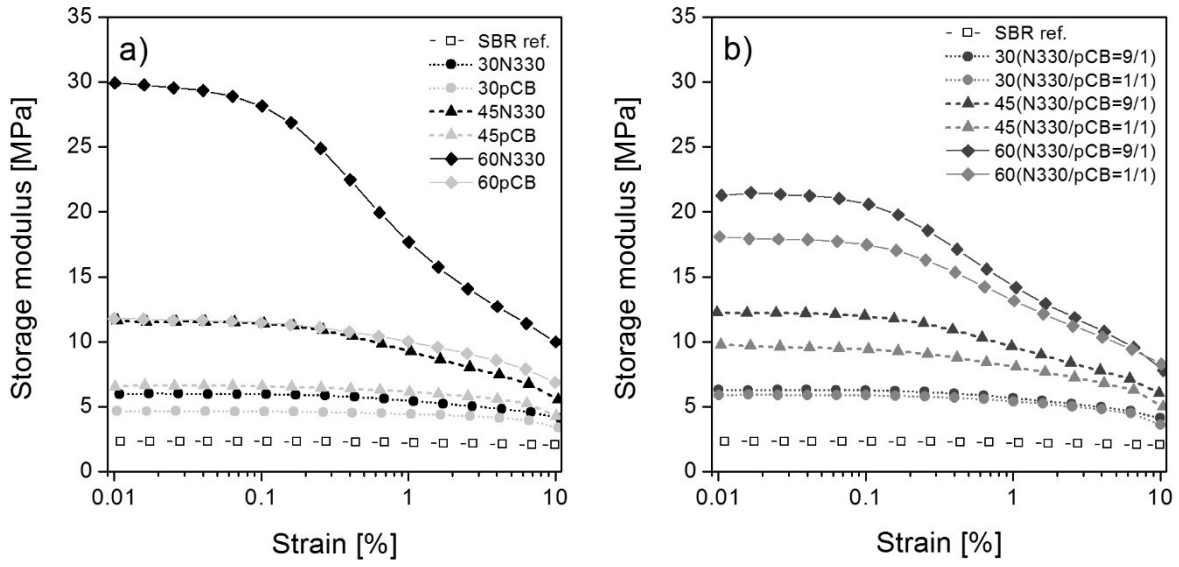

Figure 5: E' as a function of strain (Payne effect) for the SBR mixes with N330 and pCB (a) and N330+pCB (b)

Table 4: Density and DMTA-related properties of the carbon black filled SBR systems

Designation	Density [g/cm^3]	M_c (at 23 °C) [g/mol]	T_g [°C]	tan δ at T_g [1]	E'_{glassy} (T_g-30°C) [MPa]	$E'_{rubbery}$ (T_g+30°C) [MPa]	Payne effect, M0.01-M10 [MPa]	E'at 0.01 % strain (M0.01) [MPa]	E''_{max} [MPa]	E''_{max} /(M0.01-M10) [1]
SBR ref.	0.973	3445	-28.7	1.86	1655	2.5	0.34	2.3	0.32	N/A
30N330	1.087	1092	-25.7	1.22	3003	8.8	2.61	6.76	0.84	0.32
30(N330/pCB=9/1)	1.085	1133	-27.4	1.29	3104	8.9	2.2	6.3	0.89	0.40
30(N330/pCB=1/1)	1.079	1256	-26.1	1.29	3308	8.0	2.3	5.88	0.82	0.36
30pCB	1.069	1435	-27.5	1.57	2989	6.8	1.2	4.67	0.65	0.54
45N330	1.132	614	-27.7	0.96	3805	17.7	7.95	13.63	1.81	0.23
45(N330/pCB=9/1)	1.125	673	-26.4	0.98	3967	17.1	6.25	12.2	1.89	0.30
45(N330/pCB=1/1)	1.120	791	-27	1.08	3726	14.0	4.62	9.76	1.44	0.31
45pCB	1.113	1051	-27.2	1.36	3398	10.4	2.31	6.54	0.98	0.42
60N330	1.178	268	-26.4	0.7	4534	50.5	19.93	29.92	4.97	0.25
60(N330/pCB=9/1)	1.174	347	-25.9	0.74	4247	37.7	13.47	21.27	3.61	0.27
60(N330/pCB=1/1)	1.170	442	-27.6	0.87	4272	28.7	9.83	18.09	2.92	0.30
60pCB	1.165	800	-26.9	1.12	4258	17.3	4.92	11.79	1.69	0.34

3.4. Mechanical behavior

Shore A hardness increased with increasing CB content, as expected. N330 outperformed pCB in this parameter, whereas N330/pCB yielded intermediate hardness values. Tensile strength showed the same tendency – cf. Figure 6a. Tensile strain as a function of the overall CB content went through a maximum. Beyond 30 phr CB content ultimate tensile strain was markedly reduced – cf. Figure 6b. Reduction measured with the same parameters was somewhat larger with N330 (cf. Figure 6b) than with pCB, suggesting that pCB is a less active filler than N330.

The tensile properties including the moduli (i.e. strength data at 50, 100, 200 and 300% strain termed as moduli M50, M100, M200 and M300, respectively) are listed in Table 5. Note that M300/M100 represents the reinforcing efficiency of the actual filler. Data in Table 5 clearly show that the moduli increase with increasing CB content. Again, SBR with N330 exhibited higher values than with pCB and the combined use of N330/pCB delivered data in between the parent fillers. Tear strength showed an adverse trend: pCB yielded higher values than N330, and its positive effect also appeared when N330 and pCB were incorporated together (cf. Table 5). This feature, which was also observed in the case of N330/pCB combinations, can be attributed to the fact that pCB particles were larger and better dispersed than N330 particles (cf. section 3.2.)

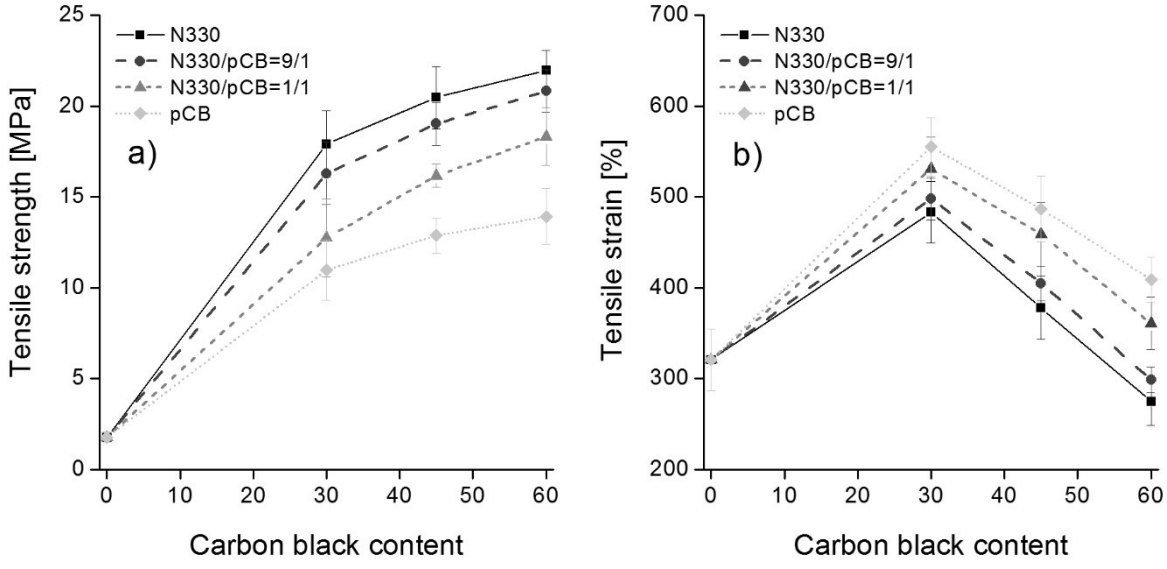

Figure 6: Tensile strength (a) and tensile strain (b) as a function of CB content for the SBR systems studied

Table 5. Hardness, tensile mechanical parameters, and tear strength for the filled SBR samples

Designation	Shore A [°]	M-50 [MPa]	M-100 [MPa]	M-200 [MPa]	M-300 [MPa]	M300/ M100 [1]	Tensile strength [MPa]	Tensile strain [%]	Tear strength [kN/m]
SBR ref.	40±1	0.6±0.0	0.8±0.0	1.2±0.0	1.7±0.1	2.1±0.1	1.78±0.3	321±34	5.36±0.1
30N330	57±1	0.9±0.2	2.0±0.1	4.6±0.2	8.9±0.2	4.5±0.4	17.91±1.8	483±34	12.00±2.0
30(N330/pCB=9/1)	56±1	1.2±0.1	1.9±0.1	2.7±0.1	7.8±0.1	4.0±0.4	16.29±1.7	498±23	11.5±1.8
30(N330/pCB=1/1)	52±1	0.9±0.2	2.8±0.0	2.9±0.6	5.3±1.0	1.9±0.3	12.75±2.1	531±35	13.39±1.0
30pCB	50±1	1.0±0.0	1.4±0.0	2.6±0.1	4.5±0.2	3.3±0.2	10.98±1.7	555±32	16.80±1.1
45N330	65±1	1.6±0.0	2.7±0.1	5.3±0.2	9.1±0.2	3.4±0.7	20.47±1.7	378±35	13.65±0.6
45(N330/pCB=9/1)	63±1	2.3±0.2	2.7±0.3	4.5±0.2	8.6±0.4	3.2±0.7	19.02±1.2	405±19	15.06±0.8
45(N330/pCB=1/1)	60±1	1.2±0.0	1.9±0.1	3.7±0.1	6.2±0.1	3.3±0.5	16.17±0.6	459±35	17.81±1.7
45pCB	57±1	1.0±0.0	1.5±0.1	2.7±0.2	4.3±0.3	2.8±0.4	12.88±1.0	487±36	20.05±1.8
60N330	74±1	1.7±0.1	3.1±0.2	8.0±0.4	14.6±0.6	4.8±0.5	21.98±1.1	275±26	17.27±1.0
60(N330/pCB=9/1)	71±1	1.6±0.1	3.0±0.2	7.6±0,3	13.8±0.3	4.7±1.1	20.82±1.2	299±14	17.73±0.9
60(N330/pCB=1/1)	69±1	1.1±0.1	1.9±0.2	4.5±0.5	8.2±0.9	4.3±0.3	18.31±1.6	361±29	25.26±2.0
60pCB	65±1	1.2±.0.0	1.9±0.1	4.1±0.2	7.2±0.2	3.8±0.3	13.92±1.5	409±25	27.80±1.0

It is noteworthy that a bimodal dispersion of fillers or a combination of fillers with different aspect ratios often resulted in improved tear strength [14, 23]. This is generally attributed to crack bifurcation phenomena associated with higher energy dissipation.

3.5. Fracture mechanics results

SBR with pCB showed slightly higher critical J-integral ($J_{critical}$) values compared to SBR with N330 – cf. Table 6. This suggests that the dispersion state of CB (mean particle size, particle distribution) affects crack onset, just like tear strength. If CB particle sizes are in a wide range, larger particle agglomerates can effectively hinder crack propagation. $J_{critical}$ was reduced by max. 20% after cylic preloading (i.e. Mullins softening) when SBR contained 60 phr CB. The lower the overall filler content in the SBR was, the less the reduction in $J_{critical}$ was.

The tearing modulus (T_J) is the slope of the J vs. CTOD function in the range of CTOD=0.1 to 0.8 mm. It increased up to 60 phr CB content. No advantage of pCB compared to N330 was noticeable considering T_J values. Cyclic preloading had a marginal effect on T_J values – cf. Table 6. By contrast, the beneficial effect of pCB is visible in the $J_{trouser}$ data – cf. Table 6. there is good correlation between tensile tear and $J_{trouser}$ values – cf. Figure 7. Similar results were published recently by Berki et. al. [14].

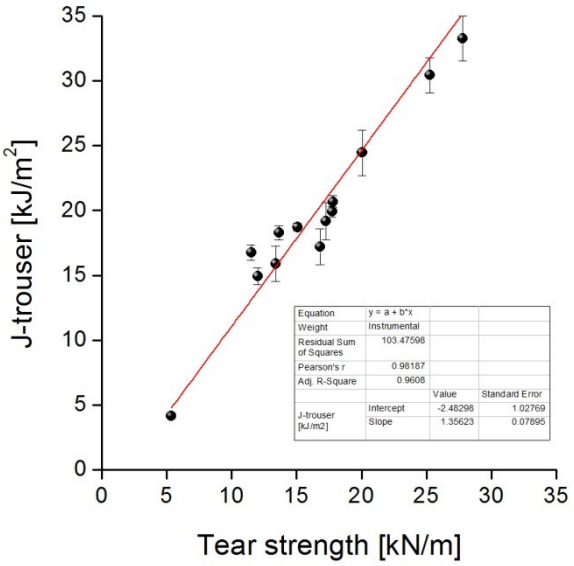

Figure 7: Correlation between tear strength and $J_{trouser}$ values of the SBR mixes

Table 6: Fracture mechanical parameters of the SBR mixes tested. Property degradation owing to preloading (Mullins effect) is indicated in percentage.

Designation	$J_{critical.\ CTOD*=0.1mm}$ [kJ/m^2]	$J_{critical.\ CTOD*=0.1mm}$ cyclically preloaded [kJ/m^2]	Tearing modulus, T_J [MJ/m^3]	Tearing modulus, T_J cyclically preloaded [MJ/m^3]	$J_{trouser}$ [kJ/m^2]
SBR ref.	0.48±0.03	0.46±0.04/ -4.17%	1.10	0.93/ -15.9%	4.2±0.2
30N330	2.60±0.10	2.46±0.45/ -5.38%	8.42	8.10/ -3.81%	14.9±0.7
30(N330/pCB=9/1)	2.63±0.24	2.46±0.03/ -6.46%	10.71	9.60/ -10.35%	16.8±0.6
30(N330/pCB=1/1)	2.71±0.10	2.52±0,05/ -7.01%	6.08	5.88/ -3.35%	15.9±1.4
30pCB	2.71±0.41	2.60±0,44/ -4.06%	4.45	4.22/ -5.22%	17.2±1.4
45N330	3.64±0.12	3.23±0,12/ -11.26%	10.17	9.86/ -3.03%	18.3±0.6
45(N330/pCB=9/1)	3.77±0.12	3.18±0,16/ -15.65%	11.37	10.29/ -9.57%	18.7±0.3
45(N330/pCB=1/1)	3.71±0.14	3.40±0,05/ -8.36%	10.41	9.79/ -5.96%	20.7±0.5
45pCB	3.98±0.60	3.70±0,58/ -7.04%	6.54	6.22/ -4.83%	24.5±1.8
60N330	4.07±0.28	3.35±0,14/ -17.69%	12.04	11.24/ -6.66%	19.2±1.4
60(N330/pCB=9/1)	3.92±0.18	3.26±0,17/ -16.84%	12.35	11.14/ -9.86%	19.9±0.4
60(N330/pCB=1/1)	4.32±0.05	3.58±0,12/ -17.13%	16.02	14.22/ -11.24%	30.4±1.4
60pCB	4.65±0.12	4.07±0,34/ -12.47%	8.93	8.39/ -6.12%	33.3±1.7

The agreement between tear strength (mode I-type loading) and $J_{trouser}$ (mode III-type loading) in Figure 7 suggests that even in the case of trouser tear mode I-type loading dominates at least in the crack tip.

3.6.Correlations

We tried to correlate tensile and fracture mechanical parameters with structure-related parameters. We selected mean molecular weight between crosslinks (M_c) as a structural parameter, which was deduced from the DMTA curves based on the rubber elasticity theory. The curve of the Payne effect and the storage modulus at the lowest measured strain (M0.01) as a function of M_c is a hyperbola – cf. Figure 8a and 8b.

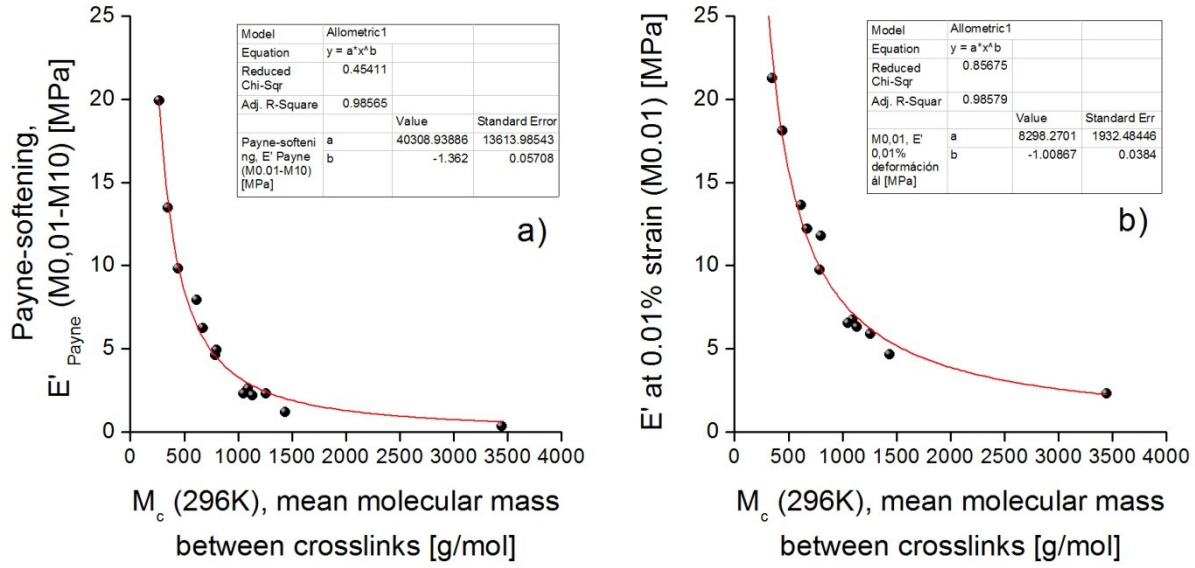

Figure 8: Plots of the Payne effect (M0.01-M10) (a) and M0.01 (b) as a function of M_c for the SBR mixes

By contrast, tensile stress changes linearly when plotted against M_c (cf. Figure 9). The $J_{critical}$ as a function of M_c (cf. Figure 10a) and even as a function of $M_c^{1/2}$ (cf. Figure 10b) show a decreasing linear trend, though with some scatter. The tearing moduli as a function of M_c and $M_c^{1/2}$, follow a decreasing trend - cf. Figure 11. Tear data vs M_c and $M_c^{1/2}$ plots behave similarly, where hardly any correlation can be found, only a decreasing tendency can be observed – cf. Figure 12. According to Lake and Thomas [24], the critical strain energy release rate changes linearly with $M_c^{1/2}$. The reason for the large scatter in the fracture mechanical parameters ($J_{critical}$, T_J, $J_{trouser}$ and tensile tear) is obviously linked with the dispersion state of (p)CB. Accordingly, it is important to quantify the dispersion characteristics of the filler and consider them along with the apparent network parameters in order to establish a more adequate description of the observed changes. There is still one open question: why did the dispersion state of the (p)CB not play a role in tensile strength? Unlike fracture parameters, which are linked to the materials' performance in a confined zone (fracture zone, path), tensile strength is a "bulk property". During tensile tests a much larger volume of the specimen is under load in which filler-caused stress concentration effects are effectively reduced via. stress homogenization in the neighborhood.

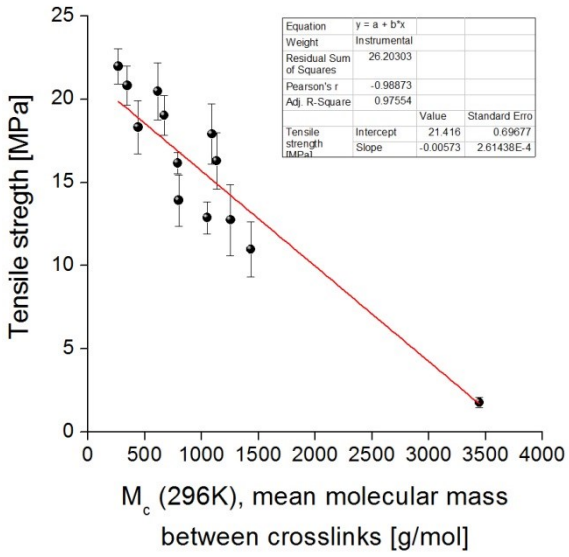

Figure 9: Tensile stress plotted against M_c for the SBR mixes

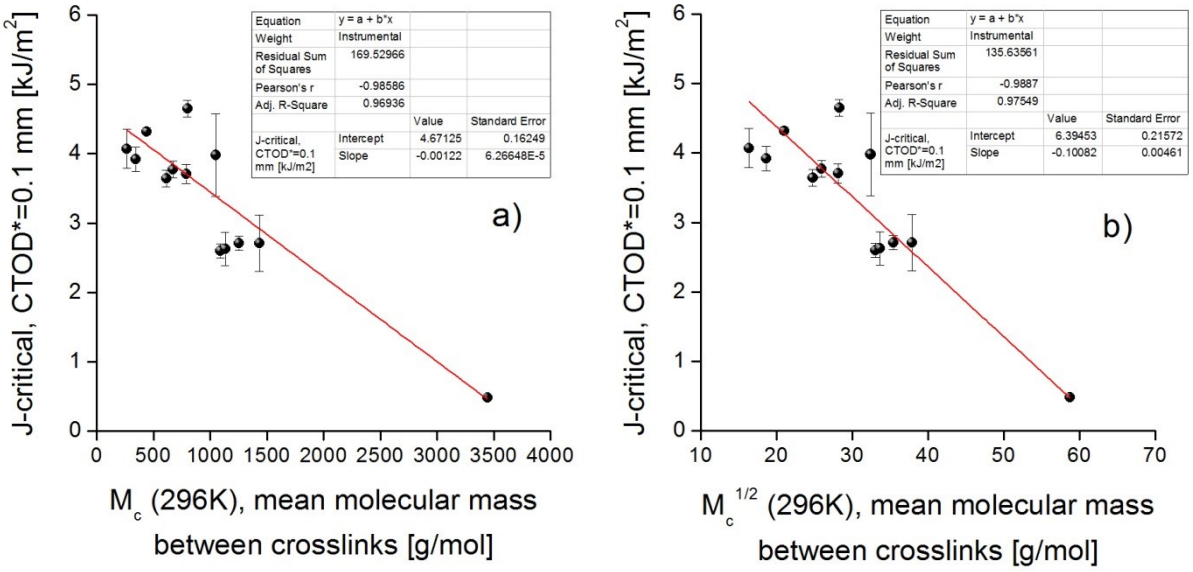

Figure 10: Critical J-integral ($J_{critical}$) plotted against M_c (a) and $M_c^{1/2}$ (b) for the SBR mixes

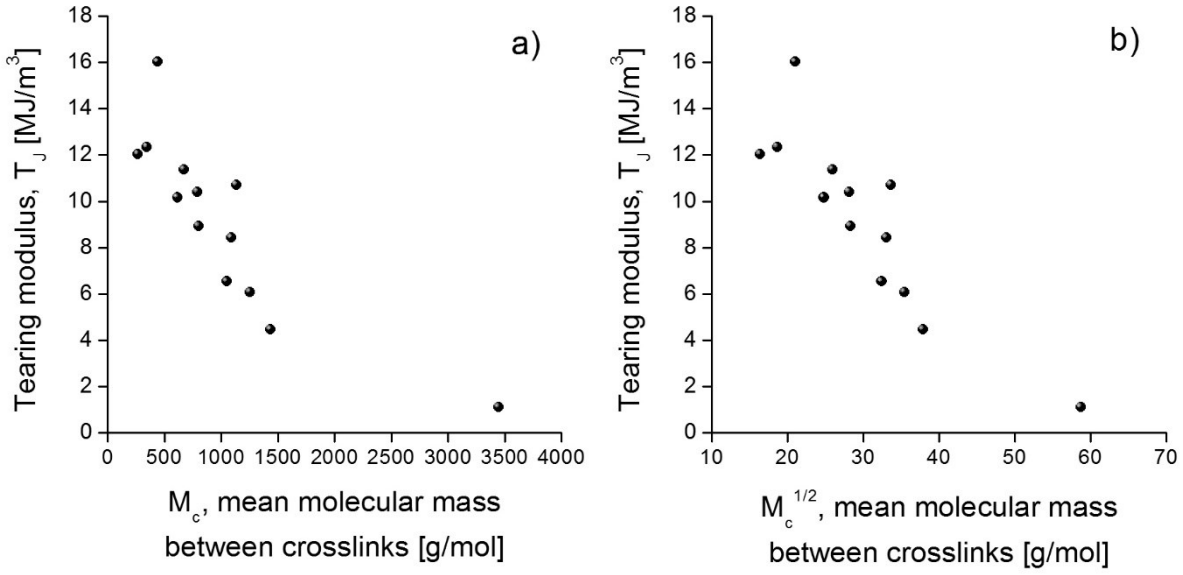

Figure 11: Tearing modulus (T_J) plotted against M_c (a) and $M_c^{1/2}$ (b) for the SBR mixes

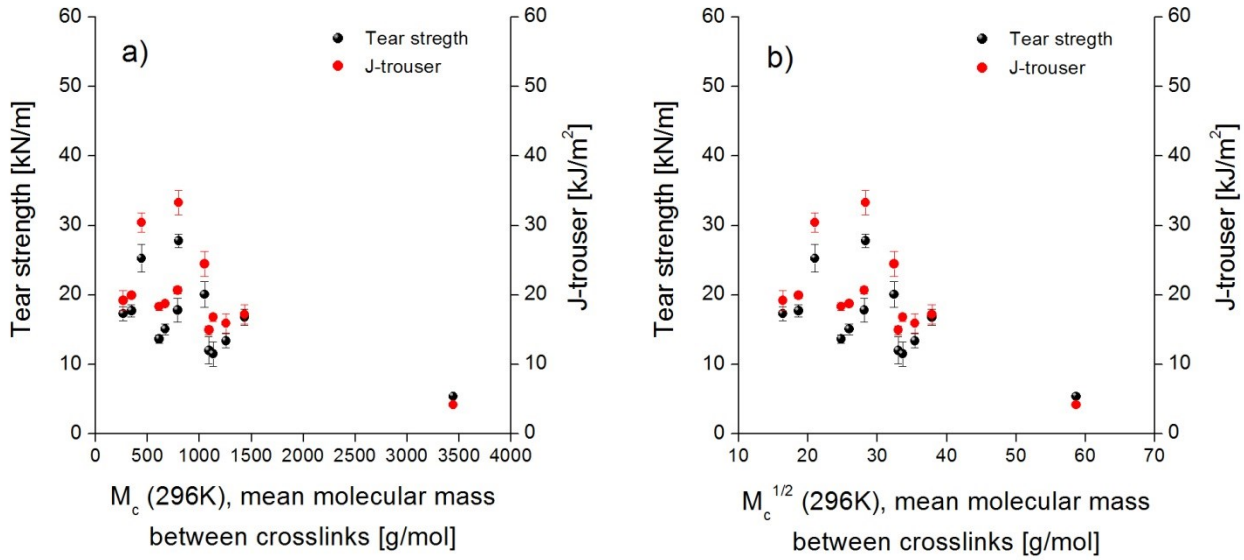

Figure 12: Tear data (tensile tear and $J_{trouser}$) plotted against M_c (a) and $M_c^{1/2}$ (b) for the SBR mixes

4. CONCLUSIONS

We set out to check the potential of pyrolytic carbon black (pCB) as reinforcing filler in SBR up to 60 phr. As a benchmark industrial N330 type CB was selected, whose specific surface area is similar to that of pCB. In order to examine the possibility of replacing N330 by pCB in more detail, we investigated N330/pCB ratios of 9/1 and 1/1. Based on the results obtained, the following conclusions can be drawn:

- adding pCB to SBR slightly affects curing compared to N330. pCB is less dispersible than N330. DMTA results showed that the industrial N330 CB is a far more active filler than pCB, suggesting that the secondary structure of CB is more important than the overall specific surface area
- N330 yielded higher tensile strength and lower elongation at break than pCB, confirming its higher reinforcing activity. Tear strength with pCB, even when combined with N330, was higher than with N330 alone. This was ascribed to pCB dispersion. Tear strength was roughly the same as trouser tear strength, suggesting that even under mode III-type loading, mode I loading dominates in the crack tip.
- pCB outperformed N330 with respect to crack initiation (J_c) and this beneficial effect also appeared when pCB and N330 were used together. It was attributed to the effect of filler dispersion, which supported efficient stress transfer/relieve locally. An opposite effect was observed for the tearing modulus (T_J), conforming that this property is influenced by CB activity
- the mechanical and fracture mechanical parameters were plotted as a function of the apparent mean molecular weight between crosslinks (M_c) and its square root ($M_c^{1/2}$). The Payne effect followed a hyperbola, whereas tensile strength and $J_{critical}$ changed linearly as a function of M_c. Scatter in the linear regression of $J_{critical}$ as a function of M_c and $M_c^{1/2}$ was attributed to filler dispersion effects. Tear parameters as a function of M_c and $M_c^{1/2}$ showed a decreasing tendency.

References:

[1] K. Formela, M. Klein, X. Colom, M.R. Saeb, Investigating the combined impact of plasticizer and shear force on the efficiency of low temperature reclaiming of ground tire rubber (GTR), Polymer Degradation and Stability, 125 (2016) 1-11.
[2] P. Lima, S.P.M. da Silva, J. Oliveira, V. Costa, Rheological properties of ground tyre rubber based thermoplastic elastomeric blends, Polymer Testing, 45 (2015) 58-67.
[3] J. Karger-Kocsis, L. Meszaros, T. Barany, Ground tyre rubber (GTR) in thermoplastics, thermosets, and rubbers, Journal of Materials Science, 48 (2013) 1-38.
[4] A. Zanchet, L.N. Carli, M. Giovanela, R.N. Brandalise, J.S. Crespo, Use of styrene butadiene rubber industrial waste devulcanized by microwave in rubber composites for automotive application, Materials and Design, 39 (2012) 437-443.
[5] P.S. Garcia, F.D.B. de Sousa, J.A. de Lima, S.A. Cruz, C.H. Scuracchio, Devulcanization of ground tire rubber: Physical and chemical changes after different microwave exposure times, Express Polymer Letters, 9 (2015) 1015-1026.
[6] S. Seghar, N.A. Hocine, V. Mittal, S. Azem, F. Al-Zohbi, B. Schmaltz, N. Poirot, Devulcanization of styrene butadiene rubber by microwave energy: Effect of the presence of ionic liquid, Express Polymer Letters, 9 (2015) 1076-1086.
[7] X. Colom, A. Faliq, K. Formela, J. Canavate, FTIR spectroscopic and thermogravimetric characterization of ground tyre rubber devulcanized by microwave treatment, Polymer Testing, 52 (2016) 200-208.
[8] J.D. Martínez, N. Puy, R. Murillo, T. García, M.V. Navarro, A.M. Mastral, Waste tyre pyrolysis – A review, Renewable and Sustainable Energy Reviews, 23 (2013) 179-213.
[9] P.T. Williams, Pyrolysis of waste tyres: A review, Waste Management, 33 (2013) 1714-1728.
[10] F. Karabork, S.T. Tipirdamaz, Influence of pyrolytic carbon black and pyrolytic oil made from used tires on the curing and (dynamic) mechanical properties of natural rubber (NR)/styrene-butadiene rubber (SBR) blends, Express Polymer Letters, 10 (2016) 72-82.

[11] Z. Jie, W. Shengji, Y. Tianming, X. Zhengmiao, Modified Pyrolytic Carbon Black from Scrap Tires and Its Reinforcement Performance in Natural Rubber, 2011 International Conference on Computer Distributed Control and Intelligent Environmental Monitoring, Changsha, China 2011, pp. 472-475.
[12] A.H. Du, M.S. Wu, C.Y. Su, H. Chen, The characterization of pyrolytic carbon black prepared from used tires and its application in styrene-butadiene rubber (SBR), Journal of Macromolecular Science Part B-Physics, 47 (2008) 268-275.
[13] C.J. Norris, M. Hale, M. Bennett, Pyrolytic carbon: factors controlling in-rubber performance, Plastics Rubber and Composites, 43 (2014) 245-256.
[14] P. Berki, J. Karger-Kocsis, Comparative Properties of Styrene-Butadiene Rubbers (SBR) Containing Pyrolytic Carbon Black, Conventional Carbon Black, and Organoclay, Journal of Macromolecular Science Part B-Physics, 55 (2016) 749-763.
[15] F. Cataldo, Preparation of pyrolytic carbon black from scrap tire rubber crumb and evaluation in new rubber compounds, Macromolecular Materials and Engineering, 290 (2005) 463-467.
[16] I.Z. Halász, T. Bárány, Novel bifunctional additive for rubbers: Cyclic butylene terephthalate oligomer, Period Polytech Mech Eng, 59 (2015) 182-188.
[17] G. Ramorino, S. Agnelli, R. De Santis, T. Ricco, Investigation of fracture resistance of natural rubber/clay nanocomposites by J-testing, Engineering Fracture Mechanics, 77 (2010) 1527-1536.
[18] S. Agnelli, G. Ramorino, S. Passera, J. Karger-Kocsis, T. Ricco, Fracture resistance of rubbers with MWCNT, organoclay, silica and carbon black fillers as assessed by the J-integral: Effects of rubber type and filler concentration, Express Polymer Letters, 6 (2012) 581-587.
[19] P. Berki, K. László, N.T. Tung, J. Karger-Kocsis, Natural rubber/graphene oxide nanocomposites via melt and latex compounding: Comparison at very low graphene oxide content, Journal of Reinforced Plastics and Composites, DOI: 10.1177/0731684417690929.
[20] B. Dong, C. Liu, L.Q. Zhang, Y.P. Wu, Preparation, fracture, and fatigue of exfoliated graphene oxide/natural rubber composites, RSC Advances, 5 (2015) 17140-17148.
[21] A.N. Gent, W.V. Mars, Strength of Elastomers, in: J.E. Mark, B. Erman, C.M. Roland (Eds.) The Science and Technology of Rubber, Academic Press, Boston, 2013, pp. 473-516.
[22] G. Heinrich, T.A. Vilgis, A statistical mechanical approach to the Payne effect in filled rubbers, Express Polymer Letters, 9 (2015) 291-299.
[23] P.L. Teh, Z.A.M. Ishak, A.S. Hashim, J. Karger-Kocsis, U.S. Ishiaku, On the potential of organoclay with respect to conventional fillers (carbon black, silica) for epoxidized natural rubber compatibilized natural rubber vulcanizates, Journal of Applied Polymer Science, 94 (2004) 2438-2445.
[24] G.J. Lake, A.G. Thomas, The Strength of Highly Elastic Materials, Proceedings of the Royal Society of London, Series A, Mathematical and Physical Sciences, 300 (1967) 108-119.